A continuum damage mechanics-based approach for the high cycle fatigue behavior of metallic polycrystals

Charles Mareau[1] and Franck Morel[1]

Abstract

Polycrystalline elasto-plasticity models provide a general framework for investigating the effect of microstructural heterogeneities (e.g. grains, inclusions, pores) on the high cycle fatigue behavior of metallic materials. In this work, continuum damage-mechanics is used to construct a set of constitutive relations to describe the progressive degradation of certain mechanical properties at the grain scale. The damage is considered to be coupled with the elastic behavior of the material. Special care is taken to include the anisotropic aspect of fatigue damage and the effect of intragranular internal stresses. The constitutive relations are then implemented within a self-consistent model to evaluate intergranular interactions. Finally, the model is used to investigate the high cycle fatigue behavior of polycrystalline copper. It is shown that the influence of certain loading conditions on the high cycle behavior is correctly reproduced. Specifically, the application of a mean shear stress does not result in an increase in damage, however a mean normal stress is damaging. That is, a decrease in the fatigue resistance is predicted when the mean normal stress is increased.

Keywords

High cycle fatigue, Crystal plasticity, Damage mechanics, Multiaxial fatigue, Metallic materials

[1]Arts et Métiers ParisTech, LAMPA, France

Corresponding author:
Charles Mareau, Arts et Métiers ParisTech, 2, boulevard du Ronceray, 49035, Angers, France.
Email: charles.mareau@ensam.eu

Introduction

For metallic materials, even though the ratio between the fatigue crack initiation life and the propagation life depends on both the material properties and the loading conditions, crack initiation is usually considered to be the dominant part of the total fatigue life in the High Cycle Fatigue (HCF) regime in the absence of large surface or volume defects. For single phase metallic alloys, fatigue crack nucleation is closely related to the localization of plastic deformation in Persistent Slip Bands (PSBs) (Broom and Summerton 1963; Klesnil and Lukas 1965; Thomson et al. 1956). As observed by Laufer and Roberts (1966), PSBs possess a characteristic structure with ladder-like dislocation arrangements being embedded in a matrix containing dipolar dislocation bundles. For metallic polycrystals, because PSBs preferably develop in grains being optimally oriented for slip (Chan 2010), the nucleation of fatigue cracks is largely influenced by crystallographic orientation (Mu et al. 2013; Signor et al. 2016).

Several attempts have been made at using polycrystalline elasto-plasticity models to describe the cyclic strain localization process leading to fatigue crack nucleation. In the context of HCF, these models can be classified into two different categories. The first category includes models that are based on an *a posteriori* approach where some indicators are computed to define whether or not the conditions for initiation and growth of a microstructurally short crack are achieved (Castelluccio and McDowell 2016; Guerchais et al. 2014; Guilhem et al. 2010; McDowell and Dunne 2010; Przybyla et al. 2010; Signor et al. 2016). The indicators, which are generally inspired by fatigue criteria (Crossland 1956; Dang Van 1973; Fatemi and Socie 1988), are calculated from stress, strain and/or energy quantities and are often space-averaged for purposes of regularization and length scale consideration (McDowell and Dunne 2010). The second category (Huyen et al. 2008; Luo and Chattopadhyay 2011; Monchiet et al. 2006; Sistaninia and Niffenegger 2014; Zghal et al. 2016) use continuum damage mechanics (Lemaitre 1996) to explicitly describe the degradation of mechanical properties. These models introduce a specific set of internal variables, that is damage variables, whose values represent the progression of fatigue damage. Though they require additional constitutive relations, damage mechanics-based models provide a natural way of evaluating the number of cycles to failure for given loading conditions.

The aim of this work is to develop a damage mechanics-based model for studying the HCF behavior of metallic polycrystals. The final objective is to evaluate the ability of such models to correctly describe the influence of different loading conditions on the development of fatigue damage. The first part of this paper is dedicated to the description of the constitutive model. It is developed at the grain scale using the general framework of crystal plasticity. The constitutive relations are then incorporated within a self-consistent model to consider the intergranular interactions associated with polycrystalline elasto-plasticity. In the second part of the paper, the proposed model is used to investigate the HCF behavior of polycrystalline copper. Special attention is given to the influence of loading conditions (e.g. mean stress state, multiaxiality, phase shift) on the development of fatigue damage.

Model description

In this section, a model for describing the development of HCF damage in metallic polycrystals is proposed. The model consists of (i) a set of constitutive equations, which are established at the grain scale, and (ii) a self-consistent method, which captures intergranular interactions. In the following, the constitutive equations, which are developed within the context of crystal plasticity, are first presented. The implementation of the constitutive relations within a self-consistent model is then detailed.

Constitutive relations

For the purpose of establishing the constitutive relations, only a single grain is considered for now. In the following, the average stress and strain states for such a grain are represented by the stress tensor $\boldsymbol{\sigma}$ and the infinitesimal strain tensor $\boldsymbol{\epsilon}$. Also, plastic deformation solely results from crystallographic slip on a set of n slip systems. In the context of crystal plasticity, each slip system α is defined using two unit vectors: the slip plane normal $\boldsymbol{n}_\alpha$ and the slip direction $\boldsymbol{m}_\alpha$. For convenience, a third unit vector $\boldsymbol{k}_\alpha = \boldsymbol{n}_\alpha \times \boldsymbol{m}_\alpha$ is introduced as well.

Composite model The cyclic behavior of metallic alloys is largely influenced by the development of intragranular dislocation structures. For instance, such structures have been observed in copper (Lukas et al. 1968; Mughrabi et al. 1979), austenitic and ferritic stainless steels (Kruml and Polák 2001; Li and Laird 1994; Li et al. 2012) and iron (Lukás and Kunz 2002). Though different spatial configurations can be adopted by the dislocations (e.g. walls and channels, cells, labyrinths), dislocation structures often consist of a soft phase (superscript s), with a low dislocation density, and a hard phase (superscript h), with a high dislocation density. For instance, for fatigued copper single crystals, the dislocation density reaches 10^{15} m^{-2} within the walls of PSBs while it is about 10^{13} m^{-2} within the channels (Grosskreutz and Mughrabi 1975; Mughrabi 1987).

The internal stress field produced by dislocation structures is often calculated from the application of homogenization theory (Langlois and Berveiller 2003; Lemoine et al. 1994; Pedersen 1990; Sauzay 2008). Indeed, following the idea of Mughrabi (1983), the intragranular dislocation structure of an individual grain can be treated as a composite material composed of a hard region, with volume fraction w, and a soft region, with volume fraction $(1 - w)$. As a result, within the general framework of homogenization theory, the stress tensor $\boldsymbol{\sigma}$ and the strain tensor $\boldsymbol{\epsilon}$ associated with a given grain are determined from the following averaging relations:

$$\boldsymbol{\sigma} = w\boldsymbol{\sigma}^h + (1 - w)\,\boldsymbol{\sigma}^s \tag{1}$$

$$\boldsymbol{\epsilon} = w\boldsymbol{\epsilon}^h + (1 - w)\,\boldsymbol{\epsilon}^s \tag{2}$$

Because the above two-phase description is adopted in the present work, the mechanical behavior of a given grain requires a set of constitutive relations for both phases and an appropriate strategy for partitioning the average stress and strain tensors between both phases. In this work, both plasticity and damage are assumed to be

controlled by the soft phase while the hard phase is given an elastic behavior. These aspects are discussed in the following paragraphs.

Soft phase For the soft phase, an elastic-plastic type of behavior is considered. Within the framework of infinitesimal transformations, the corresponding strain tensor ϵ^s is additively decomposed into an elastic contribution $\epsilon^{e,s}$ and a plastic contribution $\epsilon^{p,s}$:

$$\epsilon^s = \epsilon^{e,s} + \epsilon^{p,s} \tag{3}$$

The introduction of the elastic compliance tensor $\mathbb{S}^s$ (with the corresponding stiffness tensor $\mathbb{C}^s = \mathbb{S}^{s^{-1}}$) makes it possible to relate the elastic strain tensor to the stress tensor:

$$\epsilon^{e,s} = \mathbb{S}^s : \sigma^s \tag{4}$$

To include the influence of fatigue damage, the idea of Abdul-Latif and Saanouni (1994), which consists of introducing a damage variable d_α^s with a value between 0 and 1 for each slip system, is adopted. This concept is particularly well-suited for HCF for which the initiation of microcracks from PSBs represents an important proportion of the total fatigue life. In the present work, the elastic compliance tensor depends on the damage variables according to:

$$\mathbb{S}^s = \tilde{\mathbb{S}} + \sum_\alpha \left(\frac{d_\alpha^s}{1 - d_\alpha^s} \left(\mathrm{u}\left(\sigma_\alpha^s\right) \frac{1}{\tilde{E}_\alpha^n} \mathbb{N}_\alpha + \frac{1}{4\tilde{G}_\alpha^{mn}} \mathbb{M}_\alpha + \frac{1}{4\tilde{G}_\alpha^{kn}} \mathbb{K}_\alpha \right) \right) \tag{5}$$

where $\tilde{\mathbb{S}}$ is the initial elastic compliance tensor corresponding to an undamaged configuration, u is the unit step function* and $\sigma_\alpha^s = \boldsymbol{n}_\alpha \cdot \boldsymbol{\sigma}^s \cdot \boldsymbol{n}_\alpha$ is the normal stress acting on slip plane α. The fourth-order tensors $\mathbb{N}_\alpha$, $\mathbb{M}_\alpha$ and $\mathbb{K}_\alpha$ are defined for each slip system as follows:

$$\mathbb{N}_\alpha = \boldsymbol{n}_\alpha \otimes \boldsymbol{n}_\alpha \otimes \boldsymbol{n}_\alpha \otimes \boldsymbol{n}_\alpha \tag{6}$$

$$\mathbb{M}_\alpha = (\boldsymbol{n}_\alpha \otimes \boldsymbol{m}_\alpha + \boldsymbol{m}_\alpha \otimes \boldsymbol{n}_\alpha) \otimes (\boldsymbol{n}_\alpha \otimes \boldsymbol{m}_\alpha + \boldsymbol{m}_\alpha \otimes \boldsymbol{n}_\alpha) \tag{7}$$

$$\mathbb{K}_\alpha = (\boldsymbol{n}_\alpha \otimes \boldsymbol{k}_\alpha + \boldsymbol{k}_\alpha \otimes \boldsymbol{n}_\alpha) \otimes (\boldsymbol{n}_\alpha \otimes \boldsymbol{k}_\alpha + \boldsymbol{k}_\alpha \otimes \boldsymbol{n}_\alpha) \tag{8}$$

The initial (i.e. for an undamaged configuration) Young's modulus $\tilde{E}_\alpha^n$ as well as the shear moduli $\tilde{G}_\alpha^{mn}$ and $\tilde{G}_\alpha^{kn}$ are obtained for each slip system from the following projections:

$$\tilde{E}_\alpha^n = \left(\mathbb{N}_\alpha :: \tilde{\mathbb{S}} \right)^{-1} \tag{9}$$

$$\tilde{G}_\alpha^{mn} = \left(\mathbb{M}_\alpha :: \tilde{\mathbb{S}} \right)^{-1} \tag{10}$$

$$\tilde{G}_\alpha^{kn} = \left(\mathbb{K}_\alpha :: \tilde{\mathbb{S}} \right)^{-1} \tag{11}$$

---

*$\mathrm{u}\left(x\right) = 1$ if $x \geq 0$ and $\mathrm{u}\left(x\right) = 0$ if $x < 0$.

The main assumption behind equation (5) is that fatigue cracks initiate and propagate along slip systems. This approach is thus valid for describing the nucleation and propagation of fatigue cracks along PSBs but would be inapproppriate for some other crack initiation mechanism (e.g. inclusion cracking). Equation (5) is constructed in such a way that, when a slip system is fully damaged (i.e. $d_\alpha^s = 1$), no force can be transmitted through the corresponding slip plane, the sole exception being the case when closure effects are activated (i.e. $\sigma_\alpha^s < 0$). For this specific case, a fully damaged slip system allows transmitting forces in the normal direction n_α only. According to equation (5), the elastic compliance tensor $\mathbb{S}^s$ is necessarily symmetric and positive-definite. Also, whatever the stress state is, the continuity of the relation between the stress and elastic strain tensors is guaranteed.

To better illustrate the impact of damage on the stiffness properties, one may consider the specific case of a single slip system. For such a situation, the actual (i.e. for a possibly damaged configuration) Young's modulus E_α^n and shear moduli G_α^{mn} and G_α^{kn} are:

$$E_\alpha^n = \tilde{E}_\alpha^n \left(1 - d_\alpha^s\right)\left(1 - d_\alpha^s + d_\alpha^s \mathbf{u}\left(\sigma_\alpha^s\right)\right)^{-1} \tag{12}$$

$$G_\alpha^{mn} = \tilde{G}_\alpha^{mn} \left(1 - d_\alpha^s\right) \tag{13}$$

$$G_\alpha^{kn} = \tilde{G}_\alpha^{kn} \left(1 - d_\alpha^s\right) \tag{14}$$

The above relations emphasize the progressive decrease of the stiffness properties resulting from the development of damage.

Within the context of crystal plasticity, the plastic strain tensor is given by:

$$\epsilon^{p,s} = \frac{1}{2} \sum_\alpha \left(\mathbf{m}_\alpha \otimes \mathbf{n}_\alpha + \mathbf{n}_\alpha \otimes \mathbf{m}_\alpha\right) \gamma_\alpha^s \tag{15}$$

where γ_α^s is the plastic shear strain associated with slip system α A yield function f_α is introduced for each slip system to determine whether the conditions for plastic flow are met or not. The yield function f_α is given by:

$$f_\alpha = |\tau_\alpha^s| - r_\alpha^s \tag{16}$$

In the above equation, τ_α^s and r_α^s are respectively the resolved and critical shear stresses associated with slip system α. The resolved shear stress τ_α^s acting on the αth slip system is given by the following projection of the stress tensor:

$$\tau_\alpha^s = \mathbf{m}_\alpha \cdot \boldsymbol{\sigma}^s \cdot \mathbf{n}_\alpha \tag{17}$$

The critical shear stress r_α^s represents the resistance opposing plastic slip. For a given slip system, the resistance to plastic slip is assumed to be governed by the evolution of the corresponding dislocation density ρ_α^s. However, rather than the dislocation density ρ_α^s, an alternative variable q_α^s is introduced for each slip system to represent isotropic hardening. The internal variable q_α^s is connected to the dislocation density ρ_α^s according to the following equation:

$$q_\alpha^s = b\sqrt{\rho_\alpha^s} \tag{18}$$

where b is the norm of the Burgers vector. In the present work, a simple linear relation between the critical shear stress r_α^s and the corresponding internal variable q_α^s is assumed:

$$r_\alpha^s = Q \sum_\beta H_{\alpha\beta} q_\beta^s \tag{19}$$

where Q is the hardening modulus and the $H_{\alpha\beta}$ coefficients form a matrix that makes it possible to consider the interactions between different slip systems. The plastic shear strain rate $\dot{\gamma}_\alpha^s$ is determined from the yield function f_α with a simple viscoplastic power-law flow rule:

$$\dot{\gamma}_\alpha^s = \left(\frac{\langle f_\alpha \rangle}{K} \right)^N \operatorname{sgn}(\tau_\alpha^s) \tag{20}$$

where K and N are viscosity parameters. Also, the evolution of the isotropic hardening variable q_α^s is given by:

$$\dot{q}_\alpha^s = (1 - B q_\alpha^s) |\dot{\gamma}_\alpha^s| \tag{21}$$

where B is a material parameter characterizing the non-linearity of the isotropic hardening rule, the asymptotic value of q_α^s being $1/B$.

Following the classical approach of continuum damage mechanics (Lemaitre 1996), the driving force for damage y_α^s is given by the derivative of the elastic energy density w_e^s regarding the corresponding damage variable d_α^s. The elastic energy density w_e^s is expressed as follows:

$$w_e^s = \frac{1}{2} \boldsymbol{\sigma}^s : \mathbb{S}^s : \boldsymbol{\sigma}^s \tag{22}$$

Hence, the driving force for damage y_α^s can be written as:

$$y_\alpha^s = \frac{\partial w_e^s}{\partial d_\alpha^s} \tag{23}$$

$$= \frac{1}{2} \boldsymbol{\sigma}^s : \frac{\partial \mathbb{S}^s}{\partial d_\alpha^s} : \boldsymbol{\sigma}^s \tag{24}$$

$$= \frac{1}{2} \left(\mathbf{u}(\sigma_\alpha^s) \frac{\sigma_\alpha^{s^2}}{\tilde{E}_\alpha^n} + \frac{\tau_\alpha^{s^2}}{\tilde{G}_\alpha^{mn}} + \frac{\pi_\alpha^{s^2}}{\tilde{G}_\alpha^{kn}} \right) (1 - d_\alpha^s)^{-2} \tag{25}$$

where π_α^s is the shear stress obtained from the following projection:

$$\pi_\alpha^s = \boldsymbol{k}_\alpha \cdot \boldsymbol{\sigma}^s \cdot \boldsymbol{n}_\alpha \tag{26}$$

Expression (25) emphasizes that the development of fatigue damage on a slip plane is controlled by the joint effect of both the normal stress σ_α^s and the shear stresses τ_α^s and π_α^s. It should be noticed that the presence of the shear stress π_α^s in the definition of the driving force for damage is needed to ensure that no tangential force is transmitted in any direction for a fully damaged slip system. Also, according to the above equation, only the elastic strain energy contributes to the driving force for damage. An alternative proposition, which is not explored here, would be to include all or part of the stored energy associated with lattice defects.

By analogy with the viscoplastic flow rule (20), the evolution of the damage variable associated with the αth slip system is described with a power-law type of relation:

$$\dot{d}^s_\alpha = \left(\frac{\langle y_\alpha \rangle}{L} \right)^M (1 - d^s_\alpha) \tag{27}$$

where L and M are viscosity parameters. In the above equation, the factor $(1 - d^s_\alpha)$ is introduced to ensure that d^s_α does not exceed the maximum value of one. Because the damage evolution rule is based on a rate-dependent formalism, the present approach allows considering the possible influence of the loading frequency on the HCF behavior of metallic materials (Papakyriacou et al. 2001; Marti et al. 2015). The importance of frequency effects can be controlled with the M parameter, the specific case of $M = \infty$ corresponding to a rate-independent situation.

Hard phase For the hard phase, which occupies the dislocation rich region of the studied grain, a purely elastic behavior is assumed. This assumption is consistent with the experimental results of Tabata et al. (1982) who observed dislocations to glide much faster in the soft phase than in the hard phase in aluminium single crystals. Also, on a modelling perspective, a similar assumption is used by Sauzay (2008) to evaluate the internal stresses associated with dislocation structures. As a result, the strain tensor ϵ^h is linearly connected to the corresponding stress tensor σ^h according to:

$$\epsilon^h = \mathbb{S}^h : \sigma^h \tag{28}$$

where $\mathbb{S}^h$ (with $\mathbb{C}^h = \mathbb{S}^{h^{-1}}$) is the elastic compliance tensor. Since no damage is considered for the hard phase, the elastic compliance tensor is given by:

$$\mathbb{S}^h = \tilde{\mathbb{S}} \tag{29}$$

Voigt model To partition the strain tensor of a given grain between both phases, different strategies, usually relying on the Eshelby inclusion formalism (Langlois and Berveiller 2003; Lemoine et al. 1994; Pedersen 1990; Sauzay 2008), have been proposed. In the present work, the approach originally proposed by Mughrabi (1983), which is based on the Voigt approximation, is followed. It consists of assuming that the strain state is uniform within both phases. Thus, for a given grain, the strain tensors ϵ^h and ϵ^s associated with the hard and soft phases are:

$$\epsilon^s = \epsilon^h = \epsilon \tag{30}$$

In the original version of Mughrabi (1983), the composite model is developed for an individual slip system while a grain scale formulation is preferred in the present work. For the specific case of single slip, whether the Voigt model is applied for an individual slip system or at the granular level is not important as both strategies lead to the exact same results. However, for multiple slip, when working at the slip system level, the determination of the internal stress tensor corresponding to a given set of internal shear stresses is generally not possible. In the present work, the Voigt model is therefore applied at the granular level to avoid the aforementioned difficulties.

While the implementation of the Voigt approximation is straightforward, it completely ignores the influence of the spatial configuration adopted by dislocations. Also, because it provides an upper bound estimation of the effective behavior (Bornert et al. 2001), the adoption of the Voigt approximation generally leads to an overestimation of the internal stresses.

For a given grain, the adoption of the elastic-plastic decomposition leads to:

$$\boldsymbol{\epsilon} = \boldsymbol{\epsilon}^e + \boldsymbol{\epsilon}^p \tag{31}$$

The elastic strain tensor is determined from the elastic compliance tensor $\mathbb{S}$ as follows:

$$\boldsymbol{\epsilon}^e = \mathbb{S} : \boldsymbol{\sigma} \tag{32}$$

The effective properties of a composite grain are obtained from the application of homogenization theory (Nemat-Nasser and Hori 1998). More specifically, the averaging relations (1) and (2) together with the strain localization equation (30) allow determining the elastic stiffness tensor $\mathbb{C}$ (with $\mathbb{C} = \mathbb{S}^{-1}$):

$$\mathbb{C} = w\mathbb{C}^h + (1 - w)\,\mathbb{C}^s \tag{33}$$

The plastic strain tensor $\boldsymbol{\epsilon}^p$, which is deduced from (1), is given by:

$$\boldsymbol{\epsilon}^p = (1 - w)\,\mathbb{S} : \mathbb{C}^s : \boldsymbol{\epsilon}^{p,s} \tag{34}$$

According to the above relations, the internal stress tensor $\boldsymbol{x}^s$ associated with the soft phase, which controls the development of plasticity, is such that:

$$\boldsymbol{x}^s = \boldsymbol{\sigma} - \boldsymbol{\sigma}^s \tag{35}$$
$$= (\mathbb{I} - \mathbb{C}^s : \mathbb{S}) : \boldsymbol{\sigma} + \mathbb{C}^s : (\mathbb{I} - (1 - w)\,\mathbb{S} : \mathbb{C}^s) : \boldsymbol{\epsilon}^{p,s} \tag{36}$$

where $\mathbb{I}$ is the fourth-rank identity tensor. The above relation shows that the adoption of the Voigt approximation leads to a description of kinematic hardening which is quite similar to the linear hardening rule of Prager (1955). Indeed, when damage is not significant ($\mathbb{C}^s : \mathbb{S} \approx \mathbb{I}$), the internal stress tensor $\boldsymbol{x}^s \approx w\mathbb{C}^s : \boldsymbol{\epsilon}^{p,s}$ changes linearly with the plastic strain tensor $\boldsymbol{\epsilon}^{p,s}$.

The hard phase volume fraction w is progressively modified during a cyclic deformation process. Following the idea of Estrin et al. (1998), the evolution of the hard phase volume fraction is governed by the following evolution rule:

$$\dot{w} = A\,(W - w) \sum_{\alpha} |\dot{\gamma}^s_{\alpha}| \tag{37}$$

where W represents the asymptotic value of w and A is a material parameter controlling the evolution rate. Based on TEM observations, Evrard et al. (2010) found that the above equation provides a correct description of the hard phase volume fraction evolution in cyclic plasticity. Also, because of the development of internal stresses is directly connected to the evolution of the hard phase volume fraction, the W and A parameters govern intragranular kinematic hardening.

Self-consistent model

Because the constitutive relations have been developed at the grain scale, an appropriate method for considering the intergranular interactions resulting from the polycrystalline aspect of metallic materials is needed. In the present work, the method proposed by Mareau and Berbenni (2015), which is only briefly described here, is used. This approach aims at estimating the effective behavior of a representative volume element being formed by different constituents with an elastic-viscoplastic behavior. For the specific case of polycrystalline materials, each constituent corresponds to the set of grains sharing the same crystallographic orientation and the same shape.

The effective behavior of the representative volume element is given by the relation between the macroscopic stress rate tensor $\dot{\boldsymbol{\Sigma}}$ and the macroscopic strain rate tensor $\dot{\boldsymbol{E}}$. The macroscopic quantities $\dot{\boldsymbol{\Sigma}}$ and $\dot{\boldsymbol{E}}$ are connected to their microscopic counterparts $\dot{\boldsymbol{\sigma}}$ and $\dot{\boldsymbol{\epsilon}}$ according to:

$$\dot{\boldsymbol{\Sigma}} = \frac{1}{V} \int_V \dot{\boldsymbol{\sigma}} \, dV = \overline{\dot{\boldsymbol{\sigma}}} \tag{38}$$

$$\dot{\boldsymbol{E}} = \frac{1}{V} \int_V \dot{\boldsymbol{\epsilon}} \, dV = \overline{\dot{\boldsymbol{\epsilon}}} \tag{39}$$

The first step for the estimation of the effective behavior consists of writing the local constitutive relations in the following rate form:

$$\dot{\boldsymbol{\epsilon}} = \dot{\boldsymbol{\epsilon}}^e + \dot{\boldsymbol{\epsilon}}^p \tag{40}$$

$$= \mathbb{S} : \dot{\boldsymbol{\sigma}} + \dot{\boldsymbol{\alpha}} + \mathbb{M} : \boldsymbol{\sigma} + \dot{\boldsymbol{\beta}} \tag{41}$$

with:

$$\mathbb{S} = \frac{\partial \dot{\boldsymbol{\epsilon}}^e}{\partial \dot{\boldsymbol{\sigma}}}, \ \mathbb{C} = \mathbb{S}^{-1} \text{ and } \dot{\boldsymbol{\alpha}} = \dot{\boldsymbol{\epsilon}}^e - \mathbb{S} : \dot{\boldsymbol{\sigma}} \tag{42}$$

$$\mathbb{M} = \frac{\partial \dot{\boldsymbol{\epsilon}}^p}{\partial \boldsymbol{\sigma}}, \ \mathbb{B} = \mathbb{M}^{-1} \text{ and } \dot{\boldsymbol{\beta}} = \dot{\boldsymbol{\epsilon}}^p - \mathbb{M} : \boldsymbol{\sigma} \tag{43}$$

where $\mathbb{C}$ (respectively $\mathbb{B}$) is the elastic (respectively viscoplastic) tangent moduli tensor, $\dot{\boldsymbol{\alpha}}$ (respectively $\dot{\boldsymbol{\beta}}$) is the elastic (respectively viscoplastic) back-extrapolated strain rate.

The self-consistent approximation (Hershey 1954; Kröner 1958) is then used to obtain independent estimations of the effective properties associated with either a purely elastic or a purely viscoplastic behavior. The effective elastic stiffness tensor $\mathbb{C}^\star$ and the effective back-extrapolated strain rate $\dot{\boldsymbol{A}}^\star$ are given by the application of the self-consistent approximation to the purely elastic problem:

$$\mathbb{C}^\star = \overline{\mathbb{C} : \mathbb{A}^C} \tag{44}$$

$$\mathbb{S}^\star = \mathbb{C}^{\star-1} \tag{45}$$

$$\dot{\boldsymbol{A}}^\star = \overline{\mathbb{S}^\star : \mathbb{A}^{C^T} : \mathbb{C} : \dot{\boldsymbol{\alpha}}} \tag{46}$$

When the grains are assumed to have an ellipsoidal shape, the elastic strain localization tensor $\mathbb{A}^C$ is calculated for each constituent from the elastic Eshelby tensor $\mathbb{T}^C$ according to:

$$\mathbb{A}^C = \left(\mathbb{I} + \mathbb{T}^C : \mathbb{S}^\star : (\mathbb{C} - \mathbb{C}^\star) \right)^{-1} \tag{47}$$

In a similar fashion, the effective viscoplastic properties, which are represented by the effective viscosity tensor $\mathbb{B}^\star$ and the effective viscoplastic back-extrapolated strain rate $\dot{\boldsymbol{B}}^\star$ are obtained from the application of the self-consistent approximation to the purely viscoplastic problem:

$$\mathbb{B}^\star = \overline{\mathbb{B} : \mathbb{A}^B} \tag{48}$$

$$\mathbb{M}^\star = \mathbb{B}^{\star-1} \tag{49}$$

$$\dot{\boldsymbol{B}}^\star = \overline{\mathbb{M}^\star : \mathbb{A}^{BT} : \mathbb{B} : \dot{\boldsymbol{\beta}}} \tag{50}$$

where $\mathbb{A}^B$ is the viscoplastic strain localization tensor which depends on the viscoplastic Eshelby tensor $\mathbb{T}^B$:

$$\mathbb{A}^B = \left(\mathbb{I} + \mathbb{T}^B : \mathbb{M}^\star : (\mathbb{B} - \mathbb{B}^\star) \right)^{-1} \tag{51}$$

Finally, the solutions to the purely elastic and purely viscoplastic problems are combined to obtain the strain localization rule:

$$
\begin{aligned}
\dot{\boldsymbol{\epsilon}} = {}& \dot{\boldsymbol{E}} + \mathbb{T}^C : \left(\dot{\boldsymbol{\epsilon}}^e - \dot{\boldsymbol{A}}^\star \right) + \mathbb{T}^B : \left(\dot{\boldsymbol{\epsilon}}^p - \dot{\boldsymbol{B}}^\star \right) \\
& - \mathbb{T}^C : \mathbb{S}^\star : \mathbb{C} \left(\dot{\boldsymbol{\epsilon}}^e - \dot{\boldsymbol{\alpha}} - \mathbb{A}^C : \left(\mathbb{S}^\star : \dot{\boldsymbol{\Sigma}} + \dot{\boldsymbol{A}}^\star - \overline{\dot{\boldsymbol{\epsilon}}^e} \right) \right) \\
& - \mathbb{T}^B : \mathbb{M}^\star : \mathbb{B} : \left(\dot{\boldsymbol{\epsilon}}^p - \dot{\boldsymbol{\beta}} + \mathbb{A}^B : \left(\mathbb{M}^\star : \boldsymbol{\Sigma} + \dot{\boldsymbol{B}}^\star - \overline{\dot{\boldsymbol{\epsilon}}^p} \right) \right) \\
& + \left(\mathbb{T}^C - \mathbb{T}^B \right) : \left(\dot{\boldsymbol{\epsilon}}^p - \mathbb{A}^B : \overline{\dot{\boldsymbol{\epsilon}}^p} - \mathbb{A}^B : \mathbb{T}^B : \mathbb{M}^\star : \left(\mathbb{B} : \dot{\boldsymbol{\beta}} - \mathbb{B}^\star : \dot{\boldsymbol{B}}^\star \right) \right)
\end{aligned}
\tag{52}
$$

The above relation makes it possible to connect the local strain rate $\dot{\boldsymbol{\epsilon}}$ to the prescribed macroscopic strain rate $\dot{\boldsymbol{E}}$ without using a complex numerical procedure. Indeed, only the self-consistent solutions of the purely thermoelastic and viscoplastic heterogeneous problems are needed to estimate the interactions between the different constituents.

Application to polycrystalline copper

In this section, the proposed model is used to describe the development of HCF damage in pure polycrystalline copper. For this application, the representative volume element consists of 500 equiaxed grains with random crystallographic orientation. Crystallographic slip is assumed to occur on the twelve $\{111\}\langle110\rangle$ slip systems. In this section, the strategy used for parameter identification is first presented. Some results concerning the influence of the loading conditions are then exposed.

The stress-controlled loading conditions being examined in the following are listed in Table 1. These conditions correspond to different combinations of normal (Σ_{11}) and

Name	Normal stress Σ_{11}	Shear stress Σ_{12}
Reversed tension (Lukás and Kunz 1989)	$S_a \sin(2\pi ft)$	0
Repeated tension (Lukás and Kunz 1989)	$S_a + S_a \sin(2\pi ft)$	0
Reversed torsion (Agbessi 2013)	0	$T_a \sin(2\pi ft)$
Repeated torsion	0	$T_a + T_a \sin(2\pi ft)$
Reversed tension-torsion (in-phase) (Pejkowski et al. 2014)	$S_a \sin(2\pi ft)$	$T_a \sin(2\pi ft)$
Reversed tension-torsion (out-of-phase) (Pejkowski et al. 2014)	$S_a \sin(2\pi ft)$	$T_a \sin(2\pi ft + \pi/2)$

Table 1. List of loading conditions applied to the copper polycrystalline aggregate. The corresponding references for experimental data are also given.

shear (Σ_{12}) stresses. The loading frequency, which is denoted by f, is fixed to 10 Hz for the application of stress-controlled loading conditions.

In order to build a fracture criterion, the macroscopic damage variable D is now introduced. The macroscopic damage variable D is defined from the initial (i.e. undamaged) elastic compliance tensor $\tilde{\mathbb{S}}^\star$ and the current (i.e. damaged) stiffness tensor $\mathbb{C}^\star$ according to:

$$D = ||\mathbb{I} - \mathbb{C}^\star : \tilde{\mathbb{S}}^\star|| \tag{53}$$

For the present application, fracture is assumed to occur when the macroscopic damage variable D reaches a critical value D_c of 0.5.

Material parameters

The material parameters for copper are presented in Table 2. The strategy used to identify the model parameters is as follows. First, the elastic constants have been taken from Méric et al. (1994)[†]. For the interaction matrix H, the proposition of Asaro and Needleman (1985), which consists of distinguishing between coplanar and non-coplanar systems, is adopted. Second, the parameters associated with the viscoplastic flow rule, the isotropic hardening rule and the kinematic hardening rule (i.e. the composite model) have been determined from the different strain-controlled cyclic tests performed by Mahato et al. (2016) (see Figure 1). It should be mentioned that the initial dislocation density was assumed to be negligible so that the isotropic hardening variables q_α^s were initially assigned a zero value. Third, as shown in Figure 2, the damage-related

---

[†]For a $\{110\}\langle 111\rangle$ slip system, the corresponding Young's modulus $\tilde{E}_\alpha^n$ is 202 GPa and the shear moduli $\tilde{G}_\alpha^{mn}$ and $\tilde{G}^{kn}$ are both equal to 24.9 GPa. For comparison purposes, the effective Young's modulus $\tilde{E}^\star$ of the polycrystalline aggregate is 125 GPa and the effective shear modulus $\tilde{G}^\star$ is 46.2 GPa

Elasticity			
C_{11} (GPa)	C_{12} (GPa)	C_{44} (GPa)	
159	122	81	
Viscoplasticity			
K (MPa)	N		
32	20		
Isotropic hardening			
Q (MPa)	B	$H^{\alpha\beta}$ (coplanar)	$H^{\alpha\beta}$ (non-coplanar)
25	10	1	1.4
Kinematic hardening			
W	A		
0.05	2		
Damage			
L (MPa)	M		
0.27	6		

Table 2. Material parameters for pure copper.
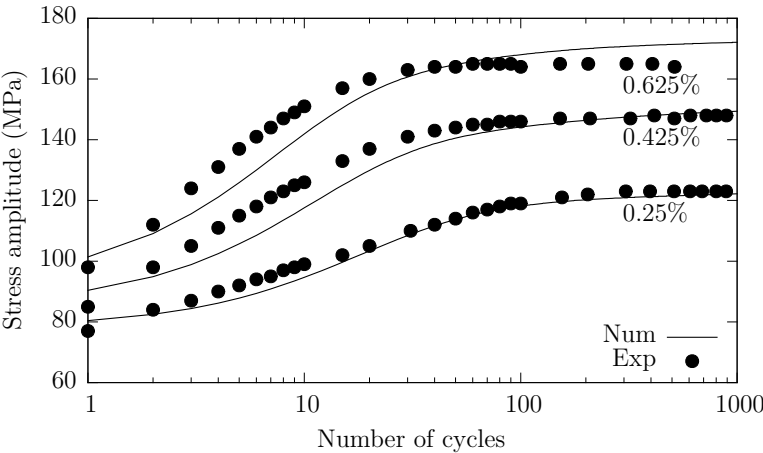
Figure 1. Evolution of the stress amplitude as a function of the number of cycles for different strain-controlled cyclic tests. The experimental results have been obtained by Mahato et al. (2016).

parameters have been adjusted to reproduce the experimental results of Lukás and Kunz (1989) who conducted fully reversed tension stress-controlled fatigue tests ($R_\sigma = -1$) on polycrystalline copper.
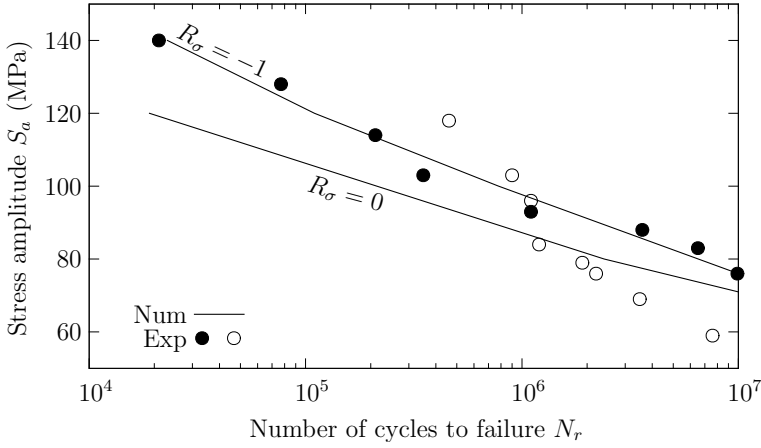
Figure 2. S-N curves for polycrystalline copper for reversed tension ($R_\sigma = -1$) and repeated tension ($R_\sigma = 0$). The experimental results have been obtained for reversed and repeated tension by Lukás and Kunz (1989).

Cyclic behavior

The macroscopic behavior of the polycrystalline aggregate for reversed tension is first discussed. The evolution of the macroscopic damage variable D as a function of the number of cycles N is plotted in Figure 3 for different stress amplitudes. The evolution of the hard phase volume fraction as a function of the number of cycles N is shown in Figure 4. For all stress amplitudes, the hard phase volume fraction tends rapidly to the asymptotic value of 5%, which is given by the W parameter. The transient regime, which corresponds to the progressive development of dislocation structures, therefore corresponds to only a small fraction of the total fatigue life. Also, according to the estimations made by Mughrabi (1983) for copper single crystals, the hard phase volume fraction is about 10% in PSBs. The hard phase volume fraction could therefore be underestimated by the present model, likely because intragranular internal stresses are not accurately evaluated with the Voigt model.

As shown in Figure 5, the progressive development of damage results in a decrease of the effective Young's modulus. Nevertheless, because of closure effects, the decrease is more significant for tension than for compression.

Influence of mean stress

The proposed model has been used to investigate the influence of mean normal and shear stresses on the HCF behavior of polycrystalline copper. As shown in Figure 6, for the case of fully reversed torsion ($R_\tau = -1$), model previsions are found to be in good agreement with the experimental data of Agbessi (2013). More specifically, the fatigue limit at 10^6
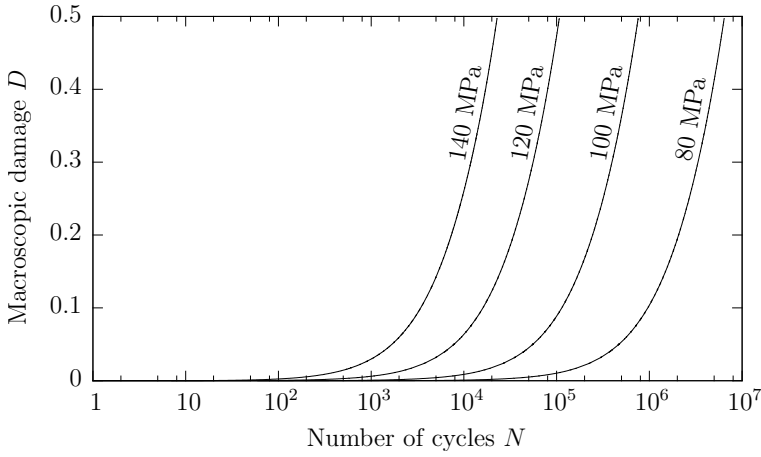
Figure 3. Evolution of the macroscopic damage variable as a function of the number of cycles for reversed tension for different stress amplitudes.
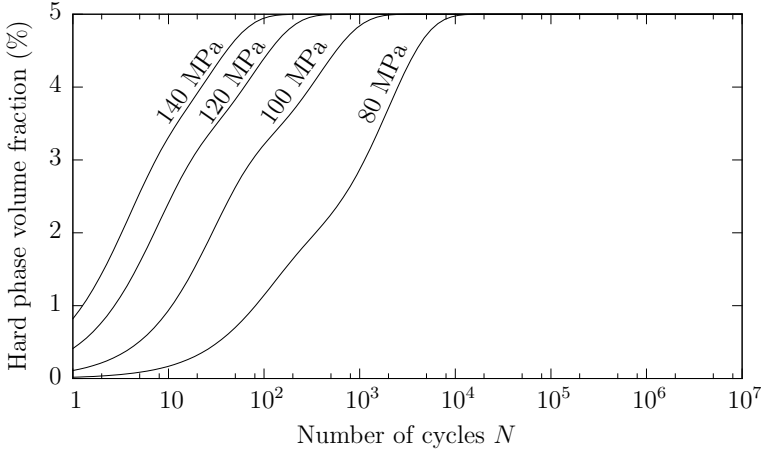

Figure 4. Evolution of the hard phase volume fraction as a function of the number of cycles for reversed tension for different stress amplitudes.

cycles, which is about 60 MPa for fully reversed torsion, is correctly predicted by the model.

Also, to evaluate the influence of the mean stress, the model predictions for repeated tension ($R_\sigma = 0$) are shown in Figure 2 together with the experimental results of Lukás and Kunz (1989). The decrease observed for the fatigue limit at 10^6 cycles for $R_\sigma = 0$ is correctly described by the model. However, the slope change observed for the S-N curve is largely underestimated by the model. Such discrepancies are possibly explained by the
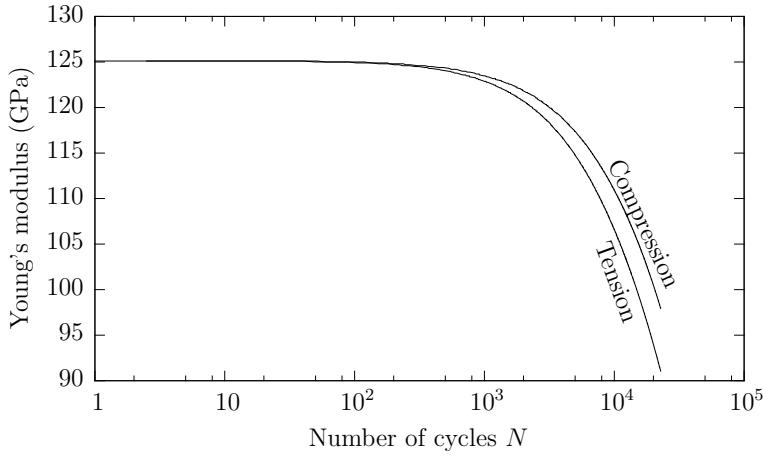
Figure 5. Evolution of the Young's modulus as a function of the number of cycles for reversed tension ($S_a = 140$ MPa).
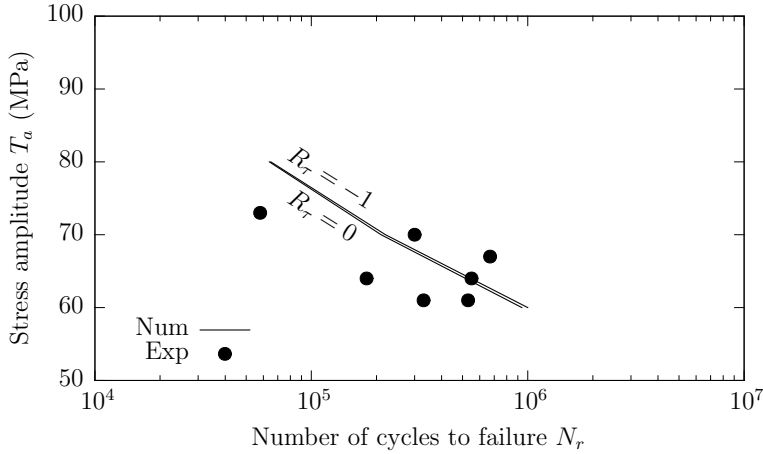
Figure 6. S-N curves for polycrystalline copper for reversed torsion ($R_\tau = -1$) and repeated torsion ($R_\tau = 0$). The experimental results have been obtained for reversed torsion by Agbessi (2013).

cross section reduction observed as a consequence of cyclic creep. Indeed, as mentioned by Lukás and Kunz (1989), the cross section reduction associated with the application of a positive mean stress may cause a progressive increase in the true stress amplitude. This aspect, which is important for high maximum stresses, is not considered in the present model as it relies on the infinitesimal deformation theory where no distinction is made between the nominal and true stresses.

The model previsions for repeated torsion ($R_\tau = 0$) are displayed in Figure 6. When comparing to the case of reversed torsion ($R_\tau = -1$), the S-N curve is almost unchanged, which is consistent with the work of (Sines 1959) who concluded that the fatigue limit of metals subjected to cyclic torsion is not affected by a superimposed mean shear stress.

It should be mentioned that differences regarding the influence of mean normal and shear stresses are correctly captured thanks to the composite model. To highlight this specific aspect, the average stress and strain tensors have been computed for the soft phase for both tension and torsion. As shown in Figure 7, the stress state of the soft phase, which governs the development of fatigue damage, is unaffected by the application of a macroscopic mean shear stress to the polycrystalline aggregate. However, the cyclic behavior of the soft phase is found to be significantly affected by the application of a macroscopic mean normal stress.

Influence of phase shift

To evaluate the influence of a phase shift on the HCF behavior of polycrystalline copper, the case of combined tension and torsion is now examined. The normalized $S_a - T_a$ diagram showing the evolution of the fatigue limit at 10^5 cycles is presented in Figure 8 for both in-phase and out-of-phase combined tension and torsion. The experimental results of Pejkowski et al. (2014), who conducted multiaxial fatigue tests on ETP copper for various T_a/S_a ratios, have been used to obtain estimations of the fatigue limit at 10^5 cycles. For in-phase loading modes, the quantitative agreement between experimental and numerical data is correct. Also, when a 90° phase shift is introduced, the beneficial influence on fatigue strength is correctly reproduced by the polycrystalline model. The beneficial effect of a phase shift is however quantitatively overestimated. This overestimation is possibly explained by the definition of the driving force for damage. According to expression (25), for a given system, the driving force y_α^s depends on the corresponding damage variable d_α^s but is independent on the other damage variables. The interactions between different damage variables are therefore not considered here though they could impact damage development, especially for non-proportional loadings. Indeed, for such loading conditions, different systems can be activated during one loading cycle and the resulting interactions may facilitate the development of fatigue damage.

Conclusions

In this work, a polycrystalline model for describing the development of HCF damage in metallic polycrystals has been proposed. The constitutive relations are written at the grain scale using the general framework of crystal plasticity. A damage variable is attached to each slip system to include the anisotropic aspect of fatigue damage. Also, a two-phase composite model is used to evaluate the internal stresses associated with the formation of intragranular dislocation structures. Constitutive relations have finally been implemented within a self-consistent model to account for intergranular interactions.

The proposed approach has been used to model the HCF behavior of a copper polycrystal. The two-phase composite model is found to be a key ingredient for capturing
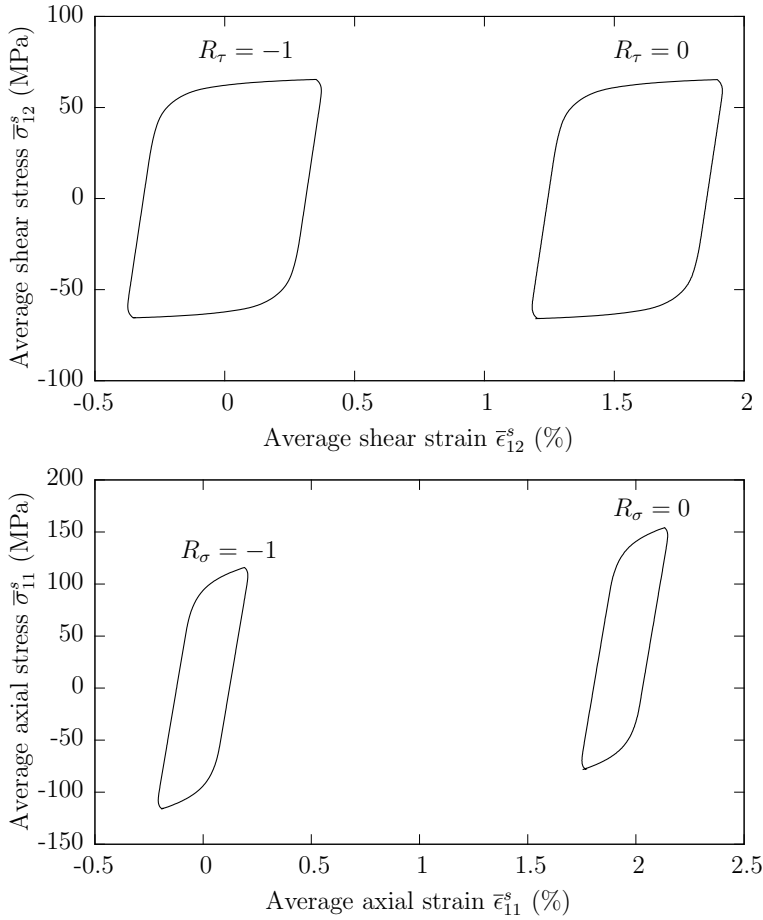
Figure 7. Cyclic behavior of the soft phase for reversed and repeated torsion ($T_a = 80$ MPa, top) and for reversed and repeated tension ($S_a = 120$ MPa, bottom). The stress-strain curves have been obtained for the 1000th loading cycle.

the effect of mean normal and shear stresses. Also, although a limited number of damage-related parameters have been introduced, the influence of a phase shift is qualitatively well reproduced. Further work should focus on the description of the interactions between damage variables. Indeed, such interactions are likely to play an important role in the development of HCF damage for complex cyclic loading paths. The extension of the proposed constitutive relations to finite strain elasto-plasticity will also be explored. This aspect is important for investigating the role of pre-straining, such as encountered in metal forming, on the HCF behavior of metallic materials.
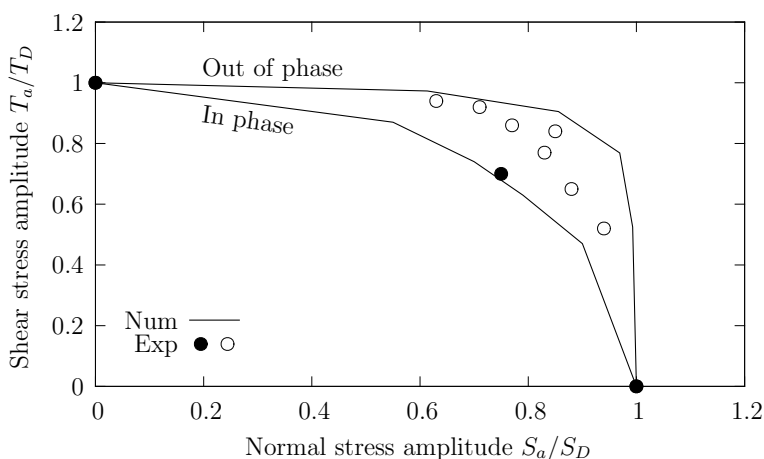
Figure 8. Evolution of the fatigue limit at 10^5 cycles for combined tension and torsion. The results of Pejkowski et al. (2014) have been used to obtain experimental estimations of the fatigue limit at 10^5 cycles.

References

Abdul-Latif A and Saanouni K (1994) Damaged Anelastic Behavior of FCC Polycrystalline Metals with Micromechanical Approach. International Journal of Damage Mechanics 3:237–259.

Agbessi K (2013) Approches expérimentales et multi-échelles des processus d'amorçage des fissures de fatigue sous chargements complexes. Phd Thesis, Ecole Nationale Supérieure d'Arts et Métiers.

Asaro RJ and Needleman A (1985) Texture development and strain hardening in rate dependent polycrystals. Acta metall. 33:923–953.

Bornert M, Bretheau T and Gilormini P (2001) Homogénéisation en mécanique des matériaux, Tome 2 : Comportements non linéaires et problèmes ouverts, Hermes science.

Broom T and Summerton JM (1963) Fatigue of zinc single crystals. Phil. Mag. 8:847–1862.

Castelluccio GM and McDowell DL (2016) Microstructure-sensitive small fatigue crack growth assessment: Effect of strain ratio, multiaxial strain state, and geometric discontinuities. International Journal of Fatigue 82:521–529.

Chan KS (2010) Roles of microstructure in fatigue crack initiation. International Journal of Fatigue 32:1428–1447.

Crossland B. Effect of large hydrostatic pressures on the torsional fatigue strength of an alloy steel. Proceedings of the International Conference on Fatigue of Metals, Institution of Mechanical Engineers, London, 1956.

Dang Van K. Sur la résistance à la fatigue des métaux. Sciences Techniques Armement 1973; 3: 47.

Estrin Y, Tóth LS, Molinari A and Bréchet Y (1998) A dislocation-based model for all hardening stages in large strain deformation. Acta mater. 46:5509–5522.

Evrard P, Alvarez-Armas I, Aubin V and Degallaix S (2010) Polycrystalline modeling of the cyclic hardening/softening behavior of an austeniticferritic stainless steel. Mechanics of Materials 42:395–404.

Fatemi A and Socie DF (1988) A critical plane approach to multiaxial fatigue damage including out-of-phase loading. Fatigue Fract Eng Mater Struct 11:14965.

Grosskreutz JC and Mughrabi H (1975) In: Argon AS (Eds.), Constitutive Equations in Plasticity. Cambridge: MIT Press, pp. 251.

Guerchais R, Robert C, Morel F and Saintier N (2014). Micromechanical study of the loading path effect in high cycle fatigue. International Journal of Fatigue 59:64–75.

Guilhem Y, Basseville S, Curtit F, Stéphan JM and Cailletaud G (2010). Investigation of the effect of grain clusters on fatigue crack initiation in polycrystals. International Journal of Fatigue 32:1748–1763.

Hershey AV (1954) The elasticity of an isotropic aggregate of anisotropic cubic crystals. Journal of Applied Mechanics 21:236–240.

Huyen N, Flacelière L and Morel F (2008) A critical plane fatigue model with coupled meso-plasticity and damage. Fatigue Fract Engng Mater Struct 31:12–28.

Klesnil M and Lukas P (1965) Dislocation arrangement in surface layer of alpha-iron grains during cyclic loading. J. Iron Steel Inst 203:1043.

Kröner E (1958) Berechnung der elastischen Konstanten des Vielkristalls aus den konstanten des Einskristalls. Zeitschrift fur Physik 151:504.

Kruml T and Polák J (2001) Fatigue softening of X10CrAl24 ferritic steel. Materials Science and Engineering A 319–321:564–568.

Langlois L and Berveiller M (2003) Overall softening and anisotropy related with the formation and evolution of dislocation cell structures. Int. J. Plast. 19:599–624.

Laufer EE and Roberts WN (1966) Dislocations and persistent slip bands in fatigued copper. Phil. Mag 14:67–78.

Lemaitre J (1996) A course on damage mechanics, 2nd ed. Berlin: Springer-Verlag Berlin Heidelberg GmbH.

Lemoine X, Muller D and Berveiller M (1994) Texture of microstructure in BCC metals for various loading paths. Mater. Sci. Forum 157–162:1821–1826.

Li Y and Laird C (1994) Cyclic response and dislocation structures of AISI 316L stainless steel. Part 1. Single crystals fatigued at intermediate strain amplitude. Materials Science and Engineering A 186:65–86.

Li Y, Aubin V, Rey C and Bompard P (2012) Polycrystalline numerical simulation of variable amplitude loading effects on cyclic plasticity and microcrack initiation in austenitic steel 304L. International Journal of Fatigue 42:71–81.

Lukas P, Knesnil M and Krejci J (1968) Dislocations and persistent slip bands in copper single crystals fatigued at low-stress amplitude. Phys. Stat. Sol. 27:545–558.

Lukás P and Kunz L (1989) Effect of mean stress on cyclic stress-strain response and high cycle fatigue life. International Journal of Fatigue 11:55–58.

Lukás P and Kunz L (2002) Cyclic plasticity and substructure of metals. Materials Science and Engineering A 322:217–227.

Luo C and Chattopadhyay A (2011) Prediction of fatigue crack initial stage based on a multiscale damage criterion. International Journal of Fatigue 33:403–413.

Mahato JK, De PS, Sarkar A, Kundu A and Chakraborti PC (2016) Grain Size Effect on LCF Behavior of Two Different FCC Metals. Procedia Engineering 160:85–92.

Mareau C and Berbenni S (2015) An affine formulation for the self-consistent modeling of elasto-viscoplastic heterogeneous materials based on the translated field method. International journal of Plasticity 64:134–150.

Marti N, Favier V, Saintier N and Gregori F (2015) Investigating fatigue frequency effects on single phase ductile materials. Procedia Engineering 133:294–298.

McDowell DL and Dunne FPE (2010) Microstructure-sensitive computational modeling of fatigue crack formation. International Journal of Fatigue 32:1521–1542.

Méric L, Cailletaud G and Gaspérini M (1994) F.E. Calculations of copper bicrystal specimens submitted to tension-compression tests. Acta Metall. Mater. 42:921–935.

Monchiet V, Charkaluk E and Kondo D (2006) Plasticity-damage based micromechanical modelling in high cycle fatigue. C. R. Mecanique 334:129–136.

Mu P, Aubin V, Alvarez-Armas I and Armas A (2013) Influence of the crystalline orientations on microcrack initiation in low-cycle fatigue. Materials Science and Engineering A 573:45–53.

Mughrabi H, Herz K and Ackermann F (1979). In: Fong JT (Eds.), Fatigue Mechanisms. Philadelphia: American Society for Testing and Materials, pp. 69.

Mughrabi H (1983) Dislocation wall and cell structures and long-range internal stresses in deformed metal crystals. Acta metall. 31:1367–1379.

Mughrabi H (1987) Long-Range Internal Stress Field in the Dislocation Wall Structure. Phys. Stat. Sol. 104:107.

Nemat-Nasser S and Hori M (1998) Micromechanics: Overall Properties of Heterogeneous Materials, 2nd ed., North Holland.

Papakyriacou M, Mayer H, Pypen C, Plenk Jr H and Stanzl-Tschegg S (2001) Influence of loading frequency on high cycle fatigue properties of b.c.c. and h.c.p. metals. Materials Science and Engineering A 308:143–152.

Pedersen OB (1990) Mechanism maps for cyclic plasticity and fatigue of single phase materials. Acta Metall. Mater. 38:1221–1239.

Pejkowski L, Skibicki D and Sempruch J (2014) High-Cycle Fatigue Behavior of Austenitic Steel and Pure Copper under Uniaxial, Proportional and Non-Proportional Loading. Journal of Mechanical Engineering 60:549–560.

Prager W (1955) The Theory of Plasticity: A Survey of Recent Achievements (James Clayton Lecture). Proc. Inst. Mech. Eng. 169:41-57.

Przybyla C, Prasannavenkatesan R, Salajegheh N and McDowell DL (2010) Microstructure-sensitive modeling of high cycle fatigue. International Journal of Fatigue 32:512–525.

Sauzay M (2008) Analytical modelling of intragranular backstresses due to deformation induced dislocation microstructures. International Journal of Plasticity 24:727–745.

Signor L, Villechaise P, Ghidossi T, Lacoste E, Gueguen M and Courtin S (2016) Influence of local crystallographic configuration on microcrack initiation in fatigued 316LN stainless steel: Experiments and crystal plasticity finite elements simulations. Materials Science and

Engineering A 649:239–249.

Sines G (1959) Behaviour of metals under complex static and alternating stresses. In: Sines G and Waisman JL (Eds.), Metal Fatigue. New-York: McGraw-Hill, pp. 14–15.

Sistaninia M and Niffenegger M (2014) Prediction of damage-growth based fatigue life of polycrystalline materials using a microstructural modeling approach. International Journal of Fatigue 66:118–126.

Stein CA, Cerrone A, Ozturk T, Le S, Kenesei P, Tucker H, Pokharel R, Lind J, Hefferan C, Suter RM, Ingraffea AR and Rollett AD (2014) Fatigue crack initiation, slip localization and twin boundaries in a nickel-based superalloy. Current Opinion in Solid State and Materials Science 18:244–252.

Tabata T, Fujita H, Hiraoka MA and Miyake S (1982) The relationship between flow stress and dislocation behaviour in [111] aluminium single crystals. Phil. Mag. A 46:801–816.

Thomson N, Wadjwer NJ and Louat N (1956) The origin of fatigue fracture in copper. Phil. Mag. 1:113.

Zghal J, Gmati H, Mareau C and Morel F (2016) A crystal plasticity based approach for the modelling of high cycle fatigue damage in metallic materials. International Journal of Damage Mechanics 25:611–628.